

Axi-Symmetric Two-Phase Suspension-Colloidal Flow in Porous Media during Water Injection

Azim Kalantariasl, Abbas Zeinijahromi, and Pavel Bedrikovetsky*

Australian School of Petroleum, University of Adelaide, Adelaide, South Australia 5005, Australia

S Supporting Information

ABSTRACT: Injection of colloids and suspensions in natural reservoirs with particle capture results in well injectivity decline. However, some initial improvement in injectivity was observed during waterflooding of oilfields and explained by increasing mobility of two-phase fluid during the displacement of more viscous oil by water. We derive an analytical model for axi-symmetric two-phase flow with simultaneous deep bed filtration of injected particles, formation of external filter cake, and its stabilization due to particle dislodgement. The explicit formula for dimensionless pressure drawdown (impedance) yields the type curve for impedance history. It is shown that the initial injectivity increase, induced by varying two-phase mobility, adds three degrees of freedom to one-phase impedance growth model. This additional information is used for tuning the models with the Corey relative permeability and the pseudo-relative permeability under the viscous-dominant displacement. Treatment of the data from three synthetic cases results in good agreement with the initial data, validating the developed model adjustment method. Three field case data have been considered. Good agreement between the field and modeling data along with common values of the obtained constants validate the developed analytical model for injectivity decline during waterflooding and its adjustment method.

1. INTRODUCTION

Decline of well injectivity has been widely observed during fresh water storage in aquifers, injection of seawater, produced water, or any poor quality water into oilfields during waterflooding, injection of solvents and polymers in oil and gas-condensate reservoirs, disposal of produced water in aquifers, cold water injection in geothermal fields, geo sequestration of CO₂ in aquifers, and industrial wastes disposal in subterranean reservoirs.^{1–9} The main physics mechanisms of the injectivity decline are capture of the particles from injected water yielding the permeability reduction (so-called deep bed filtration) and formation of low permeability external filter cake on the well wall causing further increase of the well hydraulic resistance. The above processes constitute the traditional research topics in chemical engineering. Figure 1a shows capture of injected particles in the reservoir and formation of external filter cake on the well wall. So, the decrease of well injectivity is determined by the colloidal phenomena of deep bed filtration in the reservoir rock following the formation of external filter cake.

Well injectivity is described by the injectivity index, Π , which is the well rate per unit of the pressure drop between the well and the reservoir. The normalized reciprocal to the well index is called the impedance^{6,8}

$$J(t) = \frac{\Pi(t=0)}{\Pi(t)} = \frac{q(t=0)}{\Delta p(t=0)} \frac{\Delta p(t)}{q(t)}, \quad \Delta p = p_w - p_{res} \quad (1)$$

where p is the pressure and q is the well rate. In the case of constant rate, J is the dimensionless pressure drop. Growth of the hydraulic resistance during the injection corresponds to increasing pressure drop Δp under the constant rate injection or to decreasing rate under the constant pressure drop

injection. In both cases, the well index decreases and the impedance J increases.

The mathematical model for deep bed filtration is given by the classical filtration theory.^{10–13} The analytical model of well index decline during deep bed filtration corresponds to exact solution of one-dimensional axi-symmetric suspension-colloidal flow with constant filtration coefficient and exhibits linear impedance growth with time.^{10,14–16} The schema for one-dimensional suspended transport with the following external filter cake formation is shown in Figure 1a. Formation of the external filter cake can be also described by explicit formulas that exhibit linear impedance growth under the assumptions of cake incompressibility and particle deposition layer-by-layer on the cake surface.^{14–19} The phenomena of intensive particle retention with varying filtration coefficient, small particle filtration via the external filter cake formed by larger particles, and cake compressibility, cause nonlinear growth of impedance.^{18,19} The shortcoming of the above models is unlimited impedance growth, which contradicts field observations.

Stabilization of well injectivity with time is observed in the majority of published field cases of injectivity decline.^{14,20,21} The phenomenon is explained by the dislodging of particles from the cake surface by the drag, gravitational, and lifting forces exerted on a single particle by the vertical top-down water flux in the well, while the permeate force consolidates the cake. The attracting electrostatic force in high salinity water also consolidates the cake, while it detaches the fines in low salinity brine. Figure 1b shows the particle on the top of the external

Received: June 9, 2014

Revised: September 10, 2014

Accepted: September 10, 2014

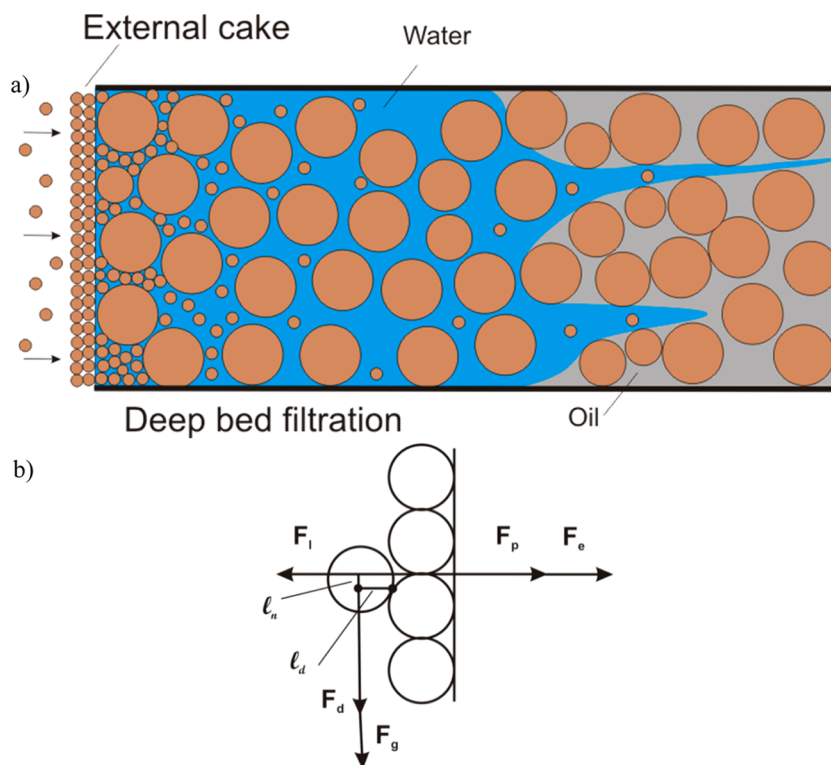


Figure 1. Four stages of injectivity impairment from the beginning of waterflooding: (a) schema of injectivity decline due to deep bed filtration and external cake formation; (b) stabilization of the external cake by erosion. Schematic for forces $F_l, k = e, p, l, d,$ and $g,$ and levers $l_m, m = n$ and $d,$ at the moment of particle dislodgment.

cake surface, the exerting forces, and their lever arms. The model for the stabilized injectivity is the torque balance of attaching and detaching forces. Verifying the model by comparison with the laboratory and well data, the authors of ref 22 show that the electrostatic forces can dominate in the torque balance; another conclusion is that the lever arm is formed by the attached particle deformation rather than by the surface asperities.

The combination of three above-mentioned injectivity stages results in monotone impedance growth with further stabilization.

However, in several field cases, it was observed that the injectivity increases from the very beginning of water injection.^{23,24} It was explained by the displacement of higher viscosity oil by water causing the timely increase of two-phase fluid mobility around the injection well.^{16,20} Figure 1a shows nonuniform displacement of oil by water causing the commingled flow of two phases at the pore scale. The areal sweep under two-phase flow at the reservoir scale is also nonuniform (Figure 2). Figure 3 shows that the retention of the particles suspended in aqueous phase causes formation damage to water. The two-phase mobility effect decreases as the displacement front propagates into the reservoir and the injectivity decline phenomena of deep bed filtration and external cake formation take over the injectivity improvement due to increasing water–oil mobility. However, the model^{16,20} exhibits unlimited impedance growth that contradicts the well history observations; also, the additional information on the initial impedance decrease is not used for improved reservoir characterization.

The present work derives an analytical model for injectivity decline with the displacement of oil by injected water during

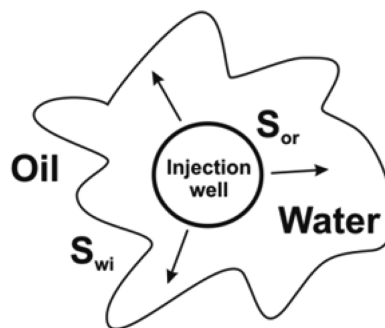


Figure 2. Schematic of viscous oil displacement by damage-free water flooding.

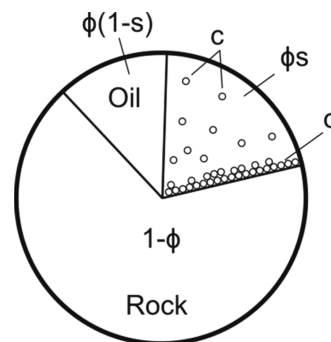


Figure 3. Schematic for filling the porous space by oil and aqueous suspension.

deep bed filtration, external cake formation, and cake stabilization stages. Introduction of cake stabilization into the model yields limited impedance values, resolving the short-

coming of the above-mentioned models. The type curve for injectivity decline is obtained from the analytical model. It is shown that consideration of two-phase displacement resulting in the initial injectivity increase adds three degrees of freedom to the traditional one-phase impedance growth model. This additional information is used for tuning the Corey relative permeability and the pseudo-relative permeability under the viscous-dominant displacement. The data for three field cases have been treated. Good agreement between the field and modeling data along with common values of the obtained constants validate the developed analytical model for injectivity decline during waterflooding and its adjustment method.

The structure of the paper is as follows: The analytical models for deep bed filtration and external cake formation are introduced in section 2. It is followed by the brief analysis of the torque balance as the injectivity stabilization model (section 3). Basic equations for two-phase colloidal-suspension flow with particle capture and formation damage are derived in section 4. Section 5 and Appendix A in Supporting Information present the impedance model for two-phase damage-free waterflooding as a particular case of the basic equations. Finally, the analytical model with the consequent separation of the coupled effects of oil–water mobility and formation damage are derived in section 6. The explicit analytical formulas allow investigating the sensitivity of well behavior to different physics effects (section 7). The history matching procedure developed in section 8 is applied to the field data treatment of three wells in section 9. Discussion of the validity of the analytical model and its wider applications for different suspension–colloidal processes concludes the paper.

2. IMPEDANCE GROWTH DURING DEEP BED FILTRATION AND EXTERNAL CAKE BUILD-UP

Following the literature,^{10,14–17,20,25,26} in the current section, we briefly describe deep bed filtration of the injected particles and external filter cake formation on the well wall resulting in well injectivity decline.

Deep particle penetration into the formation with subsequent permeability damage phenomenon is characterized by the filtration coefficient λ , which is the particle capture probability per unit length of its trajectory, and by the formation damage coefficient β , which is the increase of reciprocal to permeability per unitary concentration of the retained particles. The model assumes incompressible injected suspension, constant injected concentration, monosized particle suspension, and homogeneous rock. The assumption of low concentration for the retained particles results in constant porosity and constant filtration and formation damage coefficients. Commingled particle capture by attraction and size exclusion is considered. The analytical model shows that well impedance grows linearly versus time during the particle penetration into the reservoir^{15,27,28}

$$J_d(t_D) = 1 + mt_D, \quad m = \frac{\beta\phi c^0(\lambda r_e)^2}{2\ln \frac{r_c}{r_w}} \left(\frac{1}{\lambda r_w} + e^{\lambda r_w} \text{ei}(\lambda r_w) \right),$$

$$t_D = \frac{\int_0^t q(t) dt}{\pi r_e^2 \phi h} \quad (2)$$

where t_D is dimensionless time expressed in pore volume injected PVI, r_e is a typical half-distance between the wells (drainage radius), ϕ is porosity, h is reservoir thickness, c^0 is the

concentration of particles in the injected water, and ei is exponential integral (see ref 27 for detailed derivations).

It is assumed that at some moment, the retained concentration reaches the α -th fraction of porosity— $\alpha\phi$. The fraction α is large enough for remaining not-plugged conductive pores that are larger than the particles not to form an infinite cluster.^{15,17,28} From this transition moment on, the injected particles do not penetrate into the rock anymore while the injected carrier water does penetrate. So, the entrance reservoir cross section starts acting as an ideal filter, allowing water to pass but holding the particles in the cake. The value of the corresponding dimensionless transition time is

$$t_{tr} = \frac{2\alpha x_w}{\lambda r_w c^0}, \quad x_w = \left(\frac{r_w}{r_e} \right)^2 \quad (3)$$

The transition time is determined by the critical porosity ratio α and the filtration coefficient λ .

The external filter cake formation occurs from the transition moment onward. The cake formation model assumes incompressibility for both cake and fluid. The analytical model shows that the cake thickness is proportional to the amount of injected particles after the transition time^{15–17,20,28}

$$h_c(t_D) = \frac{\phi r_e^2 c^0 (t_D - t_{tr})}{2r_w(1 - \phi_c)} \quad (4)$$

which corresponds to the linear impedance growth

$$J_d(t_D) = 1 + mt_{tr} + m_c(t_D - t_{tr}),$$

$$m_c = \frac{kc^0\phi}{2x_w k_c(1 - \phi_c)(-\ln x_w)} \quad (5)$$

Here, k is the reservoir permeability, k_c is the permeability of external filter cake, and ϕ_c is the cake porosity.

The impedance during the cake growth can be expressed via the cake thickness by substitution of eq 4 into eq 5:

$$J_d(t_D) = 1 + mt_{tr} + m_c \frac{2r_w(1 - \phi_c)}{\phi r_e^2 c^0} h_c(t_D) \quad (6)$$

Linear impedance growth during deep bed filtration and external cake formation is shown in Figure 4 by red lines.

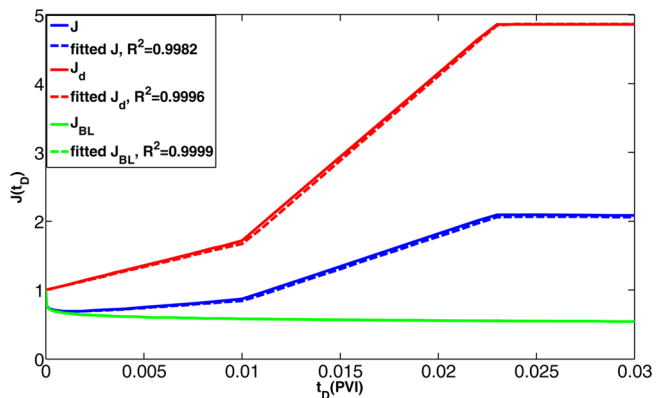


Figure 4. Treatment of first synthetic case (Table 2).

3. TORQUE BALANCE AND CAKE THICKNESS STABILIZATION

Following the literature,^{20–22} in this section, the conditions for impedance stabilization are briefly described. The stabilization of well impedance implies that the external filter cake has reached its maximum thickness. The stabilized thickness of the external cake is controlled by forces exerting on a single particle situated on the cake surface: drag (F_d), lifting (F_l), permeate (F_p), gravitational (F_g), and electrostatic forces (F_e) (Figure 1b). Here, drag force is the tangential viscous Stokes' force from the water flow along the wellbore, and permeate force is the normal viscous Stokes' force from the water flux into the formation. The expressions for these forces along with the detailed references for the values of the constants are presented in refs 8, 22, and 29.

On the cake surface, the particle attachment and consequent increase of the cake thickness occurs if torque of the attaching forces (permeate and electrostatic) exceeds torque of detaching forces (drag, lifting, and gravitational). The cake thickness increase results in increase of the hydraulic resistance to flow of injected water into formation, yielding the decrease of the permeate velocity and the subsequent decrease in the permeate force. The increase of the cake thickness leads to the decrease of the well cross section area increasing the tangential flow velocity (water flow velocity along the wellbore) and consequently increasing the drag and lifting forces. Thus, growth of external cake thickness and of the detaching torque along with declining of the attached torque occurs until reaching the torque balance:

$$(F_p + F_e - F_l)l_n = (F_d + F_g)l_d \quad (7)$$

where l_d and l_n are detaching and attaching levers, respectively. The lever arms can be obtained using the Hertz's particle deformation theory.^{12,13,22} Here, the lifting force is negligible if compared with permeate and electrostatic forces.

After the mechanical equilibrium (eq 7) is reached, the injected particles are carried with the flow along the wellbore and accumulate at the bottom of the well.

Substitution of the expressions of forces F_p , F_e , F_d , and F_g into torque balance equation (eq 7) yields an equation for stabilized cake thickness h_{cr}

$$\left(\frac{6\pi\mu_w r_s}{2\pi h(r_w - h_{cr})} 0.36 \left(\frac{k_c}{r_s^2} \right)^{-2/5} q + F_e \right) = l \left(\frac{2\omega\pi\mu_w r_s^2 q}{\pi(r_w - h_{cr})^3} + \frac{4}{3}\pi\Delta\rho g r_s^3 \right), \quad l = \frac{l_d}{l_n} \quad (8)$$

where r_s is a particle radius, $\Delta\rho$ is a density difference between particle and water, μ_w is water viscosity, and ω is the drag factor.

Substituting the obtained from eq 8 stabilized cake thickness h_{cr} into the dynamic impedance expression 6 yields the stabilized impedance value. Afterward, eq 5 gives the dimensionless stabilization moment t_e .

Finally, the impedance during the three above stages of water injection with particles is described by

$$J_d(t_D) = \begin{cases} 1 + mt_D, & t_D < t_{tr} \\ 1 + mt_{tr} + m_c(t_D - t_{tr}), & t_{tr} < t_D < t_e \\ 1 + mt_{tr} + m_c(t_e - t_{tr}), & t_D > t_e \end{cases} \quad (9)$$

The hydraulic pressure drop between the well and the reservoir is the total of those across the deep bed penetration and the cake that act as resistances in series, so the impedance additivity corresponds to the total of conductivities.

The one-phase-flow model (eq 9) contains four injectivity damage parameters: filtration coefficient λ , formation damage coefficient β , filter cake permeability k_{fc} , and lever ratio l , which can be found from well injectivity history (see refs 15–17 and 20 for detailed description of the model adjustment procedure).

Three stages of impedance growth (eq 9) are shown in Figure 4 by the red line.

4. GOVERNING EQUATIONS FOR DISPLACEMENT OF OIL BY AQUEOUS SUSPENSION

Let us derive basic equations for two-phase flow of oil and aqueous particle suspension. The detailed derivations of equations for two-phase particle-free flow can be found in refs 9 and 30; the system of one-phase suspension transport in porous media is presented in refs 10–13, 25, and 26. Solid and liquid particles are suspended in water and are transported by the velocity of the aqueous phase, so the particle retention in the rock occurs in pores saturated by water (Figures 1a and 3). The main assumptions of the model for two-phase flow of oil and aqueous particle suspension are water (aqueous suspension) and oil are immiscible; water and oil are incompressible; the suspended particles are transported by water; phase permeability for the aqueous suspension decreases with the particle retaining as a hyperbolic function of retained concentration; the particle retention rate is proportional to the advective particle flux with the constant proportionality (filtration) coefficient; particle dispersion is negligible; small retained concentration does not change the rock porosity; small suspended concentration does not change the density of water.

Under the above assumptions, the governing system for one-dimensional axi-symmetric flow consists of mass conservation for the aqueous suspension, mass conservation for both incompressible phases, generalized Darcy's law for water and oil, conservation law for suspended and retained particles and the linear kinetic expression for retaining rate:^{9,10,25,26,28–33}

$$r \frac{\partial(\phi s)}{\partial t} + \frac{\partial}{\partial r}(ru_w) = 0 \quad (10)$$

$$2\pi r h(u_w + u_o) = q(t) \quad (11)$$

$$u_w = -k \frac{k_{rw}(s)}{\mu_w(1 + \beta\sigma)} \frac{\partial p}{\partial r} \quad (12)$$

$$u_o = -k \frac{k_{ro}(s)}{\mu_o} \frac{\partial p}{\partial r} \quad (13)$$

$$r \frac{\partial(\phi sc + \sigma)}{\partial t} + \frac{\partial}{\partial r}(rcu_w) = 0 \quad (14)$$

$$\frac{\partial \sigma}{\partial t} = \lambda c u_w \quad (15)$$

Here, s is water saturation, u_w and u_o are water and oil velocities, respectively, k_{rw} and k_{ro} are relative permeability, and c and σ are suspended and retained particle concentrations.

Introduction of the fractional water flow f in the overall flux U for water and oil eqs 12 and 13 yields the following expressions for total mobility Λ and fractional flow f :

$$\Lambda(s, \sigma) = \frac{\mu_o k_{rw}(s)}{\mu_w(1 + \beta\sigma)} + k_{ro}(s) \tag{16}$$

$$f = \frac{u_w}{U} = \frac{\mu_o k_{rw}(s)}{\mu_w(1 + \beta\sigma)} \frac{1}{\Lambda(s, \sigma)} \tag{17}$$

Substituting eqs 16 and 17 into eqs 10–15 results in the following system:

$$2\pi r h \frac{\partial(\phi s)}{\partial t} + q \frac{\partial f(s, \sigma)}{\partial r} = 0 \tag{18}$$

$$U = \frac{q}{2\pi r h} = -\frac{k}{\mu_o} \Lambda(s, \sigma) \frac{\partial p}{\partial r} \tag{19}$$

$$2\pi r h \frac{\partial(\phi s c + \sigma)}{\partial t} + q \frac{\partial c f(s, \sigma)}{\partial r} = 0 \tag{20}$$

$$\frac{\partial \sigma}{\partial t} = \lambda c f U \tag{21}$$

Introduction of the following dimensionless parameters and variables in eqs 18–21

$$x_D = \left(\frac{r}{r_e}\right)^2, \quad P = \frac{4\pi k h p}{q \mu_o}, \quad C = \frac{c}{c^0}, \quad S = \frac{\sigma}{\phi c^0}, \tag{22}$$

$$\lambda_D = \lambda r_e \tag{22}$$

results in the following four dimensionless equations

$$\frac{\partial s}{\partial t_D} + \frac{\partial f(s, \sigma)}{\partial x_D} = 0 \tag{23}$$

$$1 = -x_D \Lambda(s, \sigma) \frac{\partial P}{\partial x_D} \tag{24}$$

$$\frac{\partial(sC + S)}{\partial t_D} + \frac{\partial C f(s, \sigma)}{\partial x_D} = 0 \tag{25}$$

$$\frac{\partial S}{\partial t_D} = \frac{\lambda_D C f}{2\sqrt{x_D}} \tag{26}$$

for four unknowns: saturation $s(x_D, t_D)$, suspended and retained concentrations $C(x_D, t_D)$ and $S(x_D, t_D)$, and pressure $P(x_D, t_D)$. Equation 24 separates from the system (eqs 23, 25, and 26); that is, first the unknown functions s , C , and S are determined from system (eqs 23, 25, and 26), and then, P is calculated from eq 24.

The model (eqs 23–26) describes the commingled phenomena of the displacement of oil by water and the decline in aqueous phase permeability due to capture of the injected particles. After the transition time, the displacement is occurring but the permeability profile remains intact, since no particles percolate in the reservoir anymore; the cake build-up occurs. For the case of no particle retention $\lambda = 0$, the system (eqs 23–26) degenerates into Buckley–Leverett system (eqs 23 and 24) of oil displacement by water. For the case where water saturation is equal to one, the system is reduced to a single-phase suspension transport with particle retention (eqs 24–26).

5. INJECTIVITY VARIATION DURING DAMAGE-FREE DISPLACEMENT OF OIL BY WATER

The classical Buckley–Leverett solution for one-dimensional displacement of oil by water (eq A-2; see the Appendix A, Supporting Information) allows deriving the explicit expression for impedance (eq A-4). For $M > 1$, the impedance formula (eq A-4) shows the monotone impedance decline from one at the beginning of injection to $1/M$ when time tends to infinity. The reciprocal to the mobility ratio $1/M$ can be significantly lower than one for high viscosity oils. Figure 5a shows the impedance

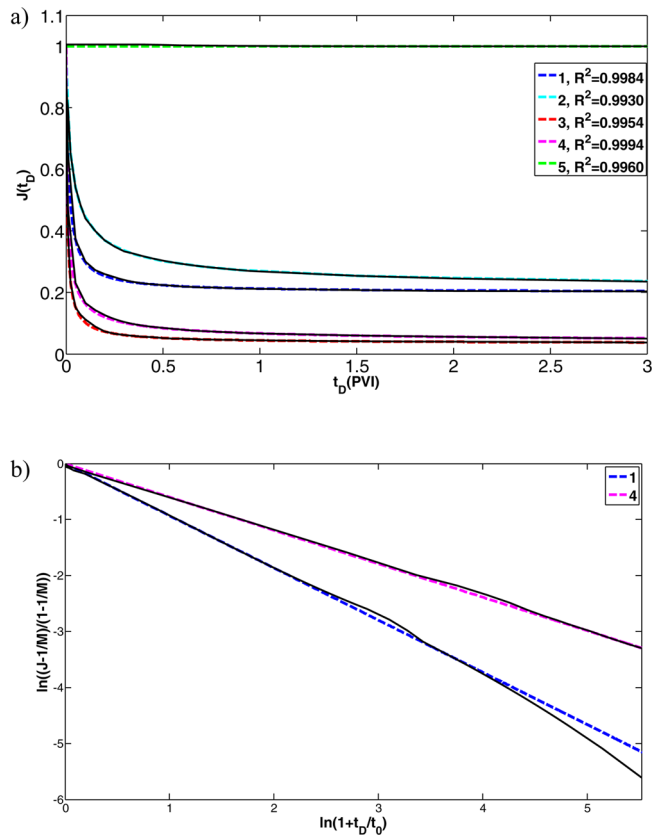


Figure 5. Approximation of damage-free impedance with power law equation: (a) from radial Buckley–Leverett solution with Corey relative phase permeability; (b) impedance for Buckley–Leverett solution and its power law approximation in log–log coordinates. The data for cases 1–5 are presented in Table 1.

decline during waterflooding for different mobility ratios $M = 1, 5,$ and 30 . Relative phase permeability $k_r(s)$ for water and oil at the core scale are described by the Corey formulas^{9,30}

$$k_{rw}(s) = k_{rwor} \left(\frac{s - s_{wi}}{1 - s_{wi} - s_{or}} \right)^{n_w}, \tag{27}$$

$$k_{ro}(s) = k_{rowi} \left(\frac{1 - s_{or} - s}{1 - s_{wi} - s_{or}} \right)^{n_o}$$

where s_{wi} is the initial water saturation, s_{or} is the residual oil saturation, k_{rwor} is relative permeability for water at $s = 1 - s_{or}$, k_{rowi} is relative permeability for oil at $s = s_{wi}$, and n_w and n_o are the powers. The Corey formulas (eq 27) usually describe concave curves of relative phase permeability; their form is determined by capillary forces. The mobility ratio M is

$$M = \frac{k_{\text{rwor}} \mu_o}{k_{\text{rowi}} \mu_w} \quad (28)$$

Five impedance waterflood curves $J_{\text{BL}}(t_{\text{D}})$ in Figure 5a are calculated for Corey parameters presented in Table 1.

Table 1. Parameters Used to Generate Damage-Free Impedance $J_{\text{BL}}(t_{\text{D}})$ and Fitted Power-Law Exponents for the Case of Corey Relative Permeability

param.	$M = 5$		$M = 30$		$M = 1$
	1	2	3	4	5
k_{rwor}	0.15	0.05	0.15	0.05	0.05
k_{rowi}	0.7	0.7	0.7	0.7	0.7
μ_o (cp)	23.33	70	140	420	14
μ_w (cp)	1	1	1	1	1
n_o	1.5	2.5	1.5	2.5	1.5
n_w	2.5	5	2.5	5	2.5
s_{wi}	0.2	0.2	0.2	0.2	0.2
s_{or}	0.3	0.3	0.3	0.3	0.3
M	5.01	5.02	30.09	30.08	1
b	-0.932	-0.578	-0.829	-0.597	
t_0 (PVI)	0.0118	0.0147	0.0043	0.0036	

Elementary volume of two-phase fluid in porous media during waterflooding is submitted to viscous, capillary, and gravitational forces. For high rate water injection in thin layer-cake reservoirs, viscous force dominates over the capillary and gravitational forces (the exact conditions for viscous dominant waterflooding in terms of dimensionless parameters can be found in refs 9, 34–36). In this case, the layers in each cross-section are filled by the displacing phase in order of decreasing of their permeability. The relative permeabilities for thin layer-cake reservoir under viscous domination are given by the following implicit formulas^{9,34,37}

$$\begin{aligned} \frac{s - s_{\text{wi}}}{1 - s_{\text{wi}} - s_{\text{or}}} &= \int_k^\infty g(k') dk', \\ k_{\text{rw}}(s) &= k_{\text{rwor}} \int_k^\infty k' g(k') dk', \\ k_{\text{ro}}(s) &= k_{\text{rowi}} \int_0^k k' g(k') dk' \end{aligned} \quad (29)$$

where $g(k)$ is the permeability distribution function. Pseudo-relative permeabilities (eq 29) are convex curves, which are typical for the reservoir scale; their form is determined by heterogeneity.

Let us show that for both cases of phase permeability (eqs 27 and 29), the damage-free impedance curve can be approximated by a three-parametric power law curve

$$J_{\text{BL}}(t_{\text{D}}) = \frac{1}{M} + \left(1 - \frac{1}{M}\right) \left(1 + \frac{t_{\text{D}}}{t_0}\right)^b, \quad b < 0 \quad (30)$$

Three adjustment parameters M , b , and t_0 are obtained by least-squares approximation of the impedance during axisymmetric displacement of oil by water. The fitted data are given by dashed curves for Corey relative permeability in Figure 5a. The values of coefficient of determination R^2 in five cases exceed 0.99, indicating good quality of matching.

For $M < 1$, the impedance curve increases with time and is also three-parametric.

Figure 5b shows the time dependency of $(J_{\text{BL}} - 1/M)/(1 - 1/M)$ given by eq 30 as plotted in logarithmic coordinates for the Corey relative phase permeability. The Buckley–Leverett impedance curves are matched by straight lines with high accuracy. The above allows concluding that the impedance curves for damage-free axis-symmetric displacement of oil by water can be approximated by the three-parametric power-law dependency (eq 30) with high accuracy. The result will be used further in section 8 to determine relative permeability from well injectivity decline history.

In the case of phase permeability for layer-cake reservoir with log-normal permeability distribution, the power-law approximation (eq 30) for impedance also has high accuracy; the coefficient of determination R^2 exceeds 0.94.

The data set for impedance values during water injection (A-4, Supporting Information) for relative permeability either eq 27 or eq 29 is three-dimensional; the rank of matrices for three independent parameters in eq 30 versus numerous impedance values $J(t_n)$, $n = 1, 2, \dots$ is equal to three.

The combined effects of impedance decline due to displacement with further impedance growth due to deep bed filtration, external cake formation and its stabilization are described by the analytical model developed in the next section.

6. INJECTIVITY CHANGE DUE TO SIMULTANEOUS EFFECT OF FORMATION DAMAGE AND VARIATION OF OIL–WATER MOBILITY

In this section, pressure drop between well and the drainage radius (A-3, Supporting Information) is calculated for asymptotic solution of the system (eqs 23–26). Let us separate the overall pressure drop across the reservoir by two terms: that between well and the damage zone boundary $x_{\text{D}} = x_{\text{d}}$ and that between the boundary $x_{\text{D}} = x_{\text{d}}$ and the drainage boundary $x_{\text{D}} = 1$:

$$\Delta P(t_{\text{D}}) = - \int_{x_w}^{x_{\text{d}}} \frac{\partial P(x_{\text{D}}, t_{\text{D}})}{\partial x_{\text{D}}} dx_{\text{D}} - \int_{x_{\text{d}}}^1 \frac{\partial P(x_{\text{D}}, t_{\text{D}})}{\partial x_{\text{D}}} dx_{\text{D}} \quad (31)$$

Since the radius of formation damage zone r_{d} is just several times larger than well radius, it is significantly smaller than the drainage radius. It allows assuming constant saturation $s = s_{\text{or}}$ in the damaged zone. The initial injectivity index is calculated for oil at the presence of initial water $s = s_{\text{wi}}$. The current injectivity index in the damaged zone is defined for water at the presence of residual oil. Therefore, the first integral term in eq 31 differs from one-phase expression eq 9 by multiplier $1/M$:

$$\begin{aligned} & - \int_{x_{\text{d}}}^{x_{\text{d}}} \frac{\partial P(x_{\text{D}}, t_{\text{D}})}{\partial x_{\text{D}}} dx_{\text{D}} \\ &= \frac{1}{M} \begin{cases} 1 + mt_{\text{D}}, & t_{\text{D}} < t_{\text{tr}} \\ 1 + mt_{\text{tr}} + m_c(t_{\text{D}} - t_{\text{tr}}), & t_{\text{tr}} < t_{\text{D}} < t_{\text{e}} \\ 1 + mt_{\text{tr}} + m_c(t_{\text{e}} - t_{\text{tr}}), & t_{\text{D}} > t_{\text{e}} \end{cases} \end{aligned} \quad (32)$$

By definition of the damaged zone radius, the retained concentration does not affect well index outside the damaged zone (see ref 27). Accounting for eq A-4, Supporting Information, the second integral term in eq 31 becomes

$$- \int_{x_{\text{d}}}^1 \frac{\partial P(x_{\text{D}}, t_{\text{D}})}{\partial x_{\text{D}}} dx_{\text{D}} = - \frac{\ln x_w}{k_{\text{rowi}}} J_{\text{BL}}(t_{\text{D}}) + \frac{\mu_w}{\mu_o k_{\text{rwor}}} \ln \frac{x_{\text{d}}}{x_w} \quad (33)$$

Substituting eqs 32 and 33 into eq 31 yields the final expression for impedance

$$J(t_D) = \begin{cases} J_{BL}(t_D) + \frac{m}{M}t_D, & t_D < t_{tr} \\ J_{BL}(t_D) + \frac{m}{M}t_{tr} + \frac{m_c}{M}(t_D - t_{tr}), & t_{tr} < t_D < t_e \\ J_{BL}(t_D) + \frac{m}{M}t_{tr} + \frac{m_c}{M}(t_e - t_{tr}), & t_D > t_e \end{cases} \quad (34)$$

where t_e is the cake thickness stabilization time, $J(t_e) = J_{cr}$.

The red line in Figure 4 corresponds to single-phase flow of particle suspension as calculated by eq 9, the green curve corresponds to the Buckley–Leverett solution (A-4, Supporting Information). The overall impedance as calculated by eq 34 is given by blue curve.

Formula 34 shows that the well impedance variation with time takes place in three stages: during deep bed filtration ($t_D < t_{tr}$), during the cake build-up period ($t_{tr} < t_D < t_e$), and after the cake thickness stabilization ($t_D > t_e$). During the deep bed filtration period, the impedance changes as a result of two simultaneous mechanisms: the damage-free displacement of low mobility oil by water and the permeability reduction due to particle capture. The additive total effect determines the shape of the well impedance curve before the transition time. During the cake build-up period, the total well impedance is the sum of the impedance for damage-free oil displacement (first term), impedance at transition time due to deep bed filtration (second term), and impedance due to external filter cake build-up (third term). The second and third terms remain constant after the external cake reaches its maximum thickness; the impedance due to displacement of oil by water continues decreasing slowly for the case $M > 1$. The total impedance slowly decreases until the falling down injected particles fill in the well column below the perforated intervals (rat hole). Afterward, the dragged down injected particles fill in well column reducing the column height and increasing the impedance.

So, the overall impedance curve is significantly non-monotone. It decreases initially due to displacement of more viscous oil by water for $M > 1$; then, it slowly increases due to deep bed filtration; afterward, it increases sharply due to external filter cake formation with the following slow decrease due to oil displacement under the stabilized cake thickness. The distinguishing type curve for well injectivity including physics description at each stage of impedance growth is extremely important during the well history interpretation.

Decoupling of injectivity decline from two-phase flow effects in the derivation of the analytical model for saturation and concentration distributions along with the pressure drawdown (eq 34) is a result of singular asymptotic expansions, where the small parameter is dimensionless filtration coefficient λr_e . The zero value of dimensionless filtration coefficient corresponds to the outer expansion (A-4, Supporting Information). The inner coordinate $(\lambda r)^2$ tends to zero as λr_e tends to zero, so the impedance history tends to that given by formula 9. Additivity of two effects in eq 34 is the consequence of independence of two expansions.

The effects of different formation damage and waterflood parameters on the type curve are analyzed in the next section.

7. SENSITIVITY STUDY

Figure 6a shows the impact of injectivity damage and varying two-phase flow mobility on the overall impedance curve; a

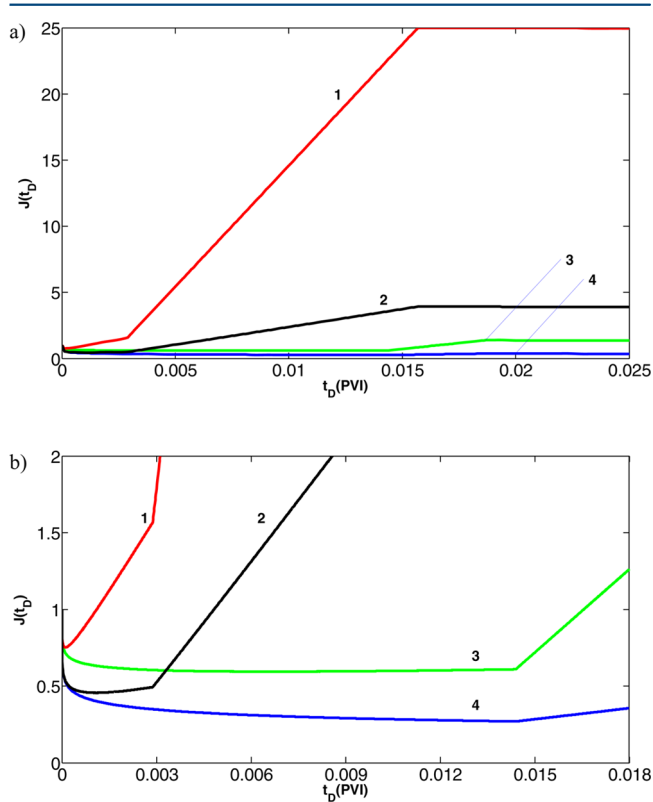


Figure 6. Three stages of well impedance growth: (a) sensitivity to mobility ratio (M) and formation damage parameters; (b) close-up for small impedance variations. The curves: 1, high injectivity damage and low mobility ratio; 2, high injectivity damage and high mobility ratio; 3, low injectivity damage and low mobility ratio; 4, low injectivity damage and high mobility ratio.

close-up for small impedance variations around the initial unitary value is presented in Figure 6b. Four cases for low and high injectivity damage as well as low and high mobility ratio M are discussed. Low damage corresponds to small filtration and formation damage coefficients and large value of external filter cake permeability. High damage corresponds to high filtration and formation damage coefficients and small value of external filter cake permeability. More specifically, high and low mobility ratios are $M = 20, 3$. Low damage parameters are $\lambda = 10$ 1/m, $\beta = 50$, $\alpha = 0.09$, $k_c = 0.1$ md, $l = 347$, $k = 1000$ md, $c^0 = 0.5$ ppm, $\phi = 0.3$, and $\phi_c = 0.2$. High damage parameters are $\lambda = 50$ 1/m, $\beta = 500$, $\alpha = 0.09$, $k_c = 0.01$ md, $l = 200$, $c^0 = 0.5$ ppm; rock and cake porosities are the same.

The first curve corresponds to high injectivity damage parameters and low mobility ratio M . The injectivity improves 1.3 times during short time $t_D = 0.0001$ and then start declining fast; the initial injectivity value is reached at the moment $t_D = 0.0011$. High damage quickly overcomes the initial injectivity increase with the displacement of light oil. The case of high damage and high mobility ratio corresponds to curve 2. From the beginning of injection, the injectivity index improves 2.1 times at the moment $t_D = 0.0005$. The initial injectivity is recovered at the moment $t_D = 0.0048$; that is, the initial

Table 2. Tuned Parameters for Three Synthetic Cases

param.	case 1			case 2			case 3		
	initial data	7 fitted params.	Corey params.	initial data	7 fitted params.	Corey params.	initial data	7 fitted params.	Corey params.
$k_{\text{rwo}}^{\text{r}}$	0.2		0.2	0.1		0.1	0.05		0.05
$k_{\text{rowi}}^{\text{r}}$	0.8		0.7850	0.65		0.6499	0.5		0.5102
μ_{o} (cp)	10		10	30		30	100		100
μ_{w} (cp)	1		1	1		1	1		1
n_{o}	1.5		1.518	1.8		1.746	2		1.890
n_{w}	3		3.006	4		4.104	5		5.040
s_{wi}	0.2		0.2	0.15		0.15	0.2		0.2
s_{or}	0.3		0.3	0.25		0.25	0.2		0.2
M	2.5	2.547		4.615	4.661		10	9.800	
b		-0.116			-0.186			-0.129	
t_0 (PVI)		1e-6			1.085e-5			1.3e-6	
β	150	144.9		300	287.4		100	99.2	
λ (m^{-1})	5	4.915		10	9.99		20	21.84	
k_{c} (md)	1	0.9890		0.3	0.3117		0.05	0.0515	
l	455	455		501	496.3		243.1	243.3	

injectivity improvement for heavy oil is higher and occurs during the longer period.

Curves 3 and 4 correspond to low formation damage cases with $M = 3$ for curve 3 and $M = 20$ for curve 4. The lower is the damage the higher is the initial injectivity gain and for the longer time it occurs.

8. HISTORY MATCHING PROCEDURE

The model given by eq 34 along with eqs 2–6 and eq 8 enables the characterization of deep bed filtration and external cake formation from well history data along with gaining some information about phase permeability, eqs 27 and 29. The injectivity decline model for a single phase flow (eq 9) is four-parametric; the independent injectivity damage parameters are the filtration and formation damage coefficients λ , β , cake permeability k_{c} , and the lever arm ratio l . Following refs 16 and 20, we assume the average value $\alpha = 0.09$ for the critical porosity ratio; this value is obtained by treatment of extensive laboratory data. As it is shown in section 5, two-phase displacement adds three parameters to the mathematical model of injectivity decline—mobility ratio M , delay time t_0 , and power b . Finally, the combined model (eq 34) has seven independent parameters. They are determined by history matching of well injectivity data.

The optimization procedure with the least-squares deviation function

$$\min_{[\lambda, \beta, k_{\text{c}}, l, M, b, t_0, t_n]} \sum_{n=1}^N [J(\lambda, \beta, k_{\text{c}}, l, M, b, t_0, t_n) - J_n]^2 \quad (35)$$

is applied. The reflective trust region algorithm for nonlinear optimization subject to bounded domains is applied for solution of the optimization problem (see ref 38). The method exhibits strong convergence. The calculations are performed by the software MatLab.³⁹

After determining the waterflood impedance constants M , t_0 , and b , the relative permeability parameters are determined. The data presented in Figure 4 and Table 2 corresponds to Corey relative phase permeability, which involves six independent constants; see eq 27. The values of end point saturations s_{wi} and s_{or} along with end point relative permeability for water $k_{\text{rwo}}^{\text{r}}$ are assumed. End point relative permeability for oil for known mobility ratio M is calculated from eq 28. Corey powers for

water and oil, n_{w} and n_{o} are determined to match power constant b and the delay time t_0 in approximation of impedance decline J_{BL} (eq 30). Three fixed values in second and fourth columns of Table 2 coincide. Three tuned parameters in second and fourth columns of Table 2 are in a good agreement. Figure 4 presents the synthetic case, where the continuous impedance curves $J(t_{\text{D}})$, $J_{\text{d}}(t_{\text{D}})$, and $J_{\text{BL}}(t_{\text{D}})$ are calculated from given constants presented in second column of Table 2. The dashed curves correspond to the adjusted model; the coefficients are presented in third and fourth columns of Table 2. The continuous and dashed curves almost coincide; the coefficient of determination R^2 exceeds 0.99. The low difference between the initial and matched parameters in the presented synthetic case is due to high accuracy approximation of the impedance waterflood curve by the power-law function. Good agreement validates the proposed model adjustment procedure.

Two other synthetic cases presented in Table 2 also have the values of the coefficient of determination exceeding 0.99.

9. RESULTS OF WELL DATA TREATMENT

In this section, the analytical model (eq 34) and associated history matching procedure (eq 35) are applied for treatment of injectivity data from three wells.

The results of data treatment based on Corey relative permeability for two wells A and B are presented in Figures 7 and 8 and in Table 3. The details about these field cases are presented in refs 23 and 24. Raw well data on rate and pressure drop have been recalculated into the impedance values, shown as blue points. The seven-parameter minimization (eq 35) has been applied. The assumed values of end points s_{wi} , s_{or} , and $k_{\text{rwo}}^{\text{r}}$ are also given in Table 3. The mobility ratio as obtained by tuning is used to calculate $k_{\text{rowi}}^{\text{r}}$ by formula 28. The powers for water and oil, n_{o} and n_{w} , are determined by least-squares minimization to match parameters b and t_0 . The obtained values of injectivity damage parameters and of Corey parameters belong to common intervals.^{8,10,15–17,20} Also, the matching quality is high: the coefficient of determination R^2 exceeds 0.92 for both cases.

Figure 9 and Table 3 show the results of case C data treatment based on pseudo-relative permeability for viscous dominant waterflooding in layer cake reservoir with log-normal permeability distribution.²⁰ The heterogeneity varies from low to moderate. The facies geometry allows assuming layer-cake

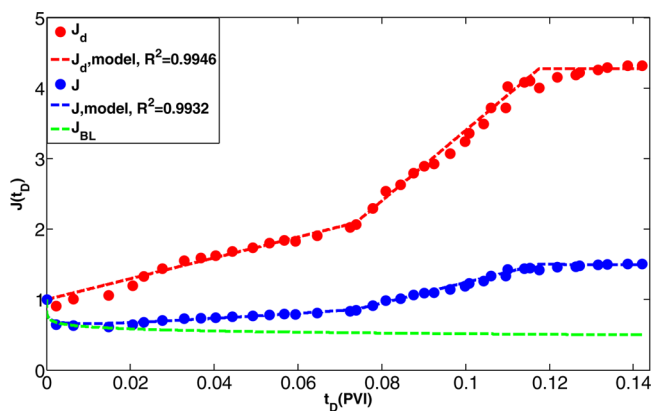


Figure 7. Treatment of water injection field data in well A (USA) using the seven-parameter optimization for Corey relative permeability.

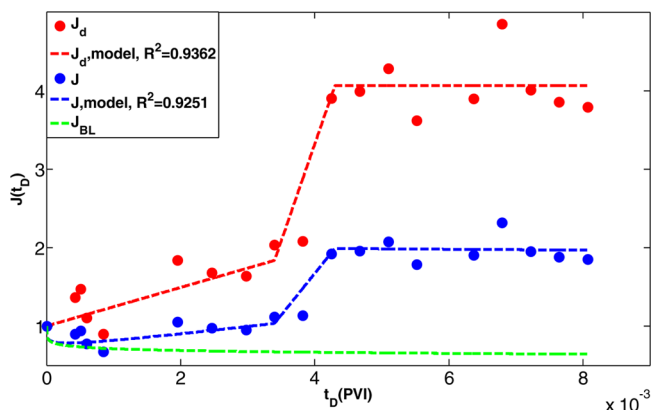


Figure 8. Treatment of water injection field data in well B (Canada) using the seven-parameter optimization for Corey relative permeability.

structure around the injection wells. Log-normal permeability distribution as obtained from breakage algorithm is typical for turbidite highly permeable sandstone reservoirs.⁴⁰ The seven-parameter minimization (eq 35) and adjustment of impedance (eq 30) are applied using pseudo-phase permeability (eq 29).

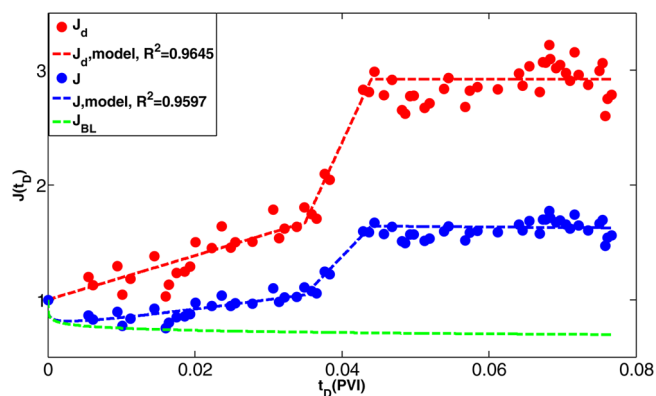


Figure 9. Treatment of water injection field data in well C (Campus Basin, Brazil) using the seven-parameter optimization for log-normal relative permeability.

As in two previous cases, high matching quality and common values of the obtained parameters take place.

10. DISCUSSION

The radius of the injectivity damage zone is significantly smaller than the drainage radius, allowing assuming the residual oil saturation in the deep bed filtration well vicinity.²⁷ It yields the splitting between nonlinear colloidal-suspension phenomena of deep bed filtration, external filter cake formation, and its stabilization from the effects of two-phase displacement. The separation results in the additivity of the well impedance due to injectivity formation damage and due to varying oil–water mobility.

The splitting yields the analytical model. The model adjustment procedure consists of the seven-parameter least-squares minimization process to find four formation damage parameters and three parameters to match the Buckley–Leverett impedance. Three parameters retrieved from the Buckley–Leverett impedance curve can be used for improved reservoir characterization. For six-parametric core-scale Corey relative permeability, the above minimization allows for choice of three constants with the following fitting of three other constants. For example, two end point saturations and relative permeability for water at the presence of residual oil can be

Table 3. Model Adjustment for Three Injection Well Histories

param.	A (U.S.A.)	B (Canada)	C (Brazil)
k_{rwor}	0.08	0.1	0.18
k_{rowi}	0.7576	0.4329	0.4356
μ_o (cp)	25	10	5
μ_w (cp)	0.8	1	1
s_{wi}	0.2	0.2	0.2
s_{or}	0.3	0.3	0.3
n_o	2.39	1.797	
n_w	4.40	3.48	
C_v			0.93
M	3.300	2.310	2.066
b	-0.1535	-0.2005	-0.1353
t_0 (PVI)	4.005×10^{-5}	4.060×10^{-5}	7.5×10^{-5}
β	697	498	173
λ (m^{-1})	4.23	7.31	0.48
k_c (md)	0.0015	0.0570	18.48
l	634	356	231

fixed, while relative permeability for oil at the presence of connate water along with two phase powers can be calculated to match three Buckley–Leverett parameters (eq 30); see the treatment of synthetic cases in section 8.

Other approaches for the model tuning can be applied depending on the available coreflood data. For example, assume that four values of end point saturations and corresponding relative permeability are known from the fast waterflood test, and the mobility ratio M is calculated from well data. The difference between the mobility ratio as obtained from the history matching and from the core data can be used to simultaneously change two end point relative permeabilities for both phases. The adjustment is important since the information came from different scales. The power b and t_0 of the waterflood impedance (eq 30) can be matched by powers n_w and n_o .

Another situation for fast end point coreflooding appears where the displacement has not been carried out long enough to establish the residual oil saturation. Usually relative permeability for water is already established while the oil drops are produced for a very long time. The assumed values are s_{wi} , $k_{r_{ow}}$ and $k_{r_{ow}}$; the powers n_w and n_o along with residual oil saturation s_{or} are the adjustment parameters.

In the case where the unsteady state coreflood has not been carrying long enough to establish residual oil saturation, the traditional Welge–JBN method for inverse problem provides the relative phase permeability for saturations below $1 - s_{or}$.^{9,30} Therefore, the values s_{wi} and $k_{r_{ow}}$ are determined with the best accuracy, the powers n_w and n_o are calculated less accurately and parameters s_{or} and $k_{r_{ow}}$ are unknown. Usually, relative permeability for water exhibits more clear power law tendency than that for oil.⁴¹ Therefore, three adjustment parameters are s_{or} , $k_{r_{ow}}$ and power n_o .

For five-parametric pseudo-phase permeability at the reservoir scale with log-normal permeability distribution (eq 29), the minimization procedure (eq 35) allows for choice of two end points with the following fitting of two end point relative phase permeability and the variance coefficient C_v .

Let us consider the case where oil and water rates along with pressure drawdown in production well are known for a long time, where water cut changes from zero up to some high value. The injectivity damage-free curve (eq 30) can be treated together with production well data. The parameters of either model 27 or model 29 can be determined from simultaneous matching of injection and production data.

The analytical model (eq 34) is developed for injection into homogeneous reservoir; see basic eqs 10–15. The typical form of relative permeability for this case is given by Corey formulas (eq 27). However, the model can be applied for the case of viscous dominant waterflooding in layer-cake reservoirs, where the pseudo-relative permeability is given by formulas in eq 29. The advanced unlimited propagation of the saturation front occurs in high permeability layers while the front delays in low permeable layers. Nevertheless, the formation damage zone during the overall displacement period almost never exceeds 1–2 m even for highly permeable layers, suggesting timely accumulation of the retained particles near wells.²⁷ The suspended concentration near to well is steady state even for layer-cake reservoir. Therefore, the retained concentration accumulates proportionally to the injected suspension volume, resulting in linear growth of the impedance (see the detailed numerical investigation in ref 42). The above supports using the averaged values of injectivity damage coefficients in close

well vicinity for the layer-cake reservoir, resulting in the averaged model (eq 34) for layer-cake reservoir submitted to viscous dominant waterflooding.

The treatment of synthetic cases with full recovery of initial coefficients validates the proposed tuning procedures.

For $M > 1$, the competitive effects of two-phase displacement and of suspension-colloidal injection result in significantly nonmonotonic typical impedance curve: the impedance decline at the beginning of injection, moderate growth during deep bed filtration, intensive growth during external filter cake formation, and slow decline after cake stabilization. The formulated impedance type curve is important for well data interpretation. It allows determining the stage of well impairment and defining well stimulation procedures.

Ignoring the collective effects of two-phase displacement and of suspension injection may result in wrong interpretation of well injectivity history. Let us consider the case where the well injectivity test shows that after some time of water injection the injectivity index is equal to the initial index: one may conclude that the injectivity remains constant during the injection; that is, the injectivity impairment does not occur. Figure 6b shows that, on the contrary, fast impedance growth occurs after the well testing. If at some moment during the displacement of heavy oil the injectivity index is equal to its initial value, the initial injectivity gain is compensated by the intensive formation damage; this formation damage takes over when the displacement front is far away from the injection well and oil mobility does not affect the well index anymore; fast injectivity decline follows. All curves in Figure 6 show the impedance increase after the moment t_1 , when the initial and current injectivities are equal: $J(t_1) = 1$.

Consider the situation where the model is fitted to the injectivity data from the beginning of injection up to some moment shortly after the stabilization time t_e . The obtained parameters can be used for further behavior prediction of the same well. The parameters can be also used for injectivity prediction for new wells, completed in the same or similar reservoir. The matched injectivity history can be also implemented into numerical reservoir simulator for improved reservoir characterization accounting for injectivity decline.

Different damage mechanisms can be responsible for permeability impairment and subsequent injectivity decline. The proposed analytical model cannot distinguish the mechanism of injectivity decline due to formation damage from well injectivity data. Further, additional evidence is required to diagnosis the dominant mechanism during deep bed filtration. Injectivity can also be impaired by fines lifting, migration, and straining, by biological clogging, by sulphate scaling, etc.⁶ The above processes are outside the scope of the current paper. However, if the impedance curve of the well has the type form discussed in section 6 (Figures 4, 6–9) and the tuned values of formation damage and two-phase flow parameters belong to the common intervals, it allows claiming that the injectivity impairment occurs due to injection of water with particles. This conclusion is important for decision making on injected water treatment technology or on well stimulation.

If compared with the analytical model (eq 34), numerical models simulate water injection into significantly more complex reservoirs.^{43,44} However, the analytical model allows formulating the well-posed inverse problem for tuning of seven parameters with further arbitrary choice of the remaining constants. Inverse solution of ill-posed numerical problem is

significantly more cumbersome and does not solve the problem of uniqueness of the solution.

Significant injectivity damage is observed during injection of CO₂ and N₂, foam injection,^{45–47} polymer flooding and some other methods of enhanced recovery,^{9,30,48,49} cold water injection into geothermal reservoirs,^{4,5} injection of fresh water in unsaturated subterranean storages,^{1–3} etc. The above processes are described by two-phase multicomponent axisymmetric flows and allow for self-similar solution similar to eq A-2, Supporting Information.^{9,30} The splitting between the effects of injected suspension and the effects of two-phase multicomponent displacements (eqs 31–34) yields the analytical model similar to that developed for waterflooding. The splitting can be performed even if the waterflooding solution is semianalytical, such as for water injection into fractured-porous formations.⁵⁰

The analytical model (eqs 8 and 34) can be also applied for prediction of the stabilized external cake during drilling. Along with the formulas for deep bed filtration and external filter cake formation under two-phase displacement, the model (eq 34) can be used for prediction of the drilling fluid invasion into the formation, which is important for interpretation of electric logging data.^{51,52}

11. CONCLUSIONS

Derivation of the analytical model of oil displacement by aqueous particle suspension and treatment of the field data allows drawing the following conclusions:

- Two simultaneous mechanisms of the formation damage due to particle capture and oil–water mobility variation are competitive: deep bed filtration, external cake formation, and its stabilization yield the decrease in injectivity, while the displacement of high viscosity oil by water ($M > 1$) results in well injectivity increase.
- The competition results in significantly nonmonotonic impedance type curve: the impedance declines at the beginning of injection; the moderate growth during deep bed filtration follows; the intensive growth during external filter cake formation occurs afterward; and slow decline takes place after cake stabilization for $M > 1$. For $M < 1$, the impedance keeps increasing monotonically after the stabilization.
- Introduction of the damaged zone radius, which has order of magnitude of well radius and is significantly smaller than the drainage radius, allows separating the formation damage effect from that of the two-phase flow: the effect of the retained particles captured outside the damaged zone on well injectivity is negligible, while oil saturation inside the damaged zone is almost equal to residual oil saturation.
- The separation leads to the analytical model of deep bed filtration, external cake formation, and its stabilization during the displacement of oil by water.
- The impedance for two-phase damage-free displacement allows for high accuracy approximation by three-parametric power-law function.
- Consideration of varying oil–water mobility during the displacement adds three degrees of freedom to the impedance curve if compared with the four-parametric single-phase injectivity decline model. Three additional numbers can be used for improved reservoir character-

ization, determining the relative permeability, or describing the permeability distribution.

- A good match of the field data by the mathematical model as well as the obtained model constants that vary in common intervals validates the developed analytical model and the seven-parameter tuning procedure.

■ ASSOCIATED CONTENT

📄 Supporting Information

Appendix A: Calculation of Damage Free Injectivity Index Due to Mobility Variation (Buckley–Leverett Solution). This material is available free of charge via the Internet at <http://pubs.acs.org>

■ AUTHOR INFORMATION

Corresponding Author

*Email: pavel@asp.adelaide.edu.au

Notes

The authors declare no competing financial interest.

■ ACKNOWLEDGMENTS

The authors thank Australian Research Council (DP1094299 and LP100100613) and Santos Ltd. for generous sponsorship. Many thanks are due to Dr. Z. You (Australian School of Petroleum) for help with numerical simulation.

■ NOMENCLATURE

- b = power-law exponent
- c^0 = concentration of particles in the injected water, ppm
- c = suspended particle concentration, ppm
- C = dimensionless suspended particle concentration
- f = fractional flow of water
- F_d = drag force, MLT^{-2} , N
- F_e = electrostatic force, MLT^{-2} , N
- F_g = gravitational force, MLT^{-2} , N
- F_l = lifting force, MLT^{-2} , N
- F_p = permeate force, MLT^{-2} , N
- $g(k)$ = permeability distribution function
- h = reservoir thickness, L, m
- h_c = external cake thickness, L, m
- h_{cr} = critical (stabilized) external cake thickness, L, m
- Π = injectivity index, L^4TM^{-1} , $\text{m}^4 \text{ s kg}^{-1}$
- J = impedance
- J_{BL} = damage-free impedance
- J_{cr} = critical (stabilized) well impedance
- J_d = impedance due to formation damage
- k = reservoir permeability, L^2 , m^2
- k_c = external cake permeability, L^2 , m^2
- k_{ro} = oil phase relative permeability
- k_{rwor} = oil phase relative permeability at initial water saturation
- k_{rw} = water phase relative permeability
- k_{rwor} = water relative permeability at residual oil saturation
- l = lever arm ratio
- l_d = lever arm for tangential forces, L, m
- l_n = lever arm for normal forces, L, m
- M = mobility ratio
- m = slope of impedance growth during deep bed filtration
- m_c = slope of impedance growth during cake formation
- n_o = Corey power for oil phase
- n_w = Corey power for water phase
- p = pressure, $\text{ML}^{-1} \text{ T}^{-2}$, Nm^{-2}

p_w = wellbore pressure, $\text{ML}^{-1} \text{T}^{-2}$, Nm^{-2}
 p_{res} = reservoir pressure, $\text{ML}^{-1} \text{T}^{-2}$, Nm^{-2}
 P = dimensionless pressure
 q = water injection rate, $\text{L}^3 \text{T}^{-1}$, $\text{m}^3 \text{s}^{-1}$
 r_d = damaged zone radius, L , m
 r_e = reservoir radius, L , m
 r_s = particle radius, L , m
 r_w = wellbore radius, L , m
 s = water saturation
 S = dimensionless retained particle concentration
 s_f = saturation of water front
 s_{or} = residual oil saturation
 s_{wi} = initial water saturation
 t = time, T , s
 t_0 = delay time (PVI)
 t_D = dimensionless time (PVI)
 t_e = dimensionless stabilization time (PVI)
 t_{tr} = dimensionless transition time (PVI)
 U = overall flux, LT^{-1} , m s^{-1}
 u_o = oil phase velocity, LT^{-1} , m s^{-1}
 u_w = water phase velocity, LT^{-1} , m s^{-1}
 x_d = dimensionless squared damaged zone radius
 x_D = dimensionless squared radius
 x_w = dimensionless squared well radius

Greek Letters

α = critical porosity fraction
 β = formation damage coefficient
 λ = filtration coefficient, L^{-1} , m^{-1}
 λ_D = dimensionless filtration coefficient
 μ_o = oil viscosity, $\text{ML}^{-1}\text{T}^{-1}$, $\text{kg m}^{-1}\text{s}^{-1}$
 μ_w = water viscosity, $\text{ML}^{-1}\text{T}^{-1}$, $\text{kg m}^{-1}\text{s}^{-1}$
 σ = retained particle concentration
 ΔP = dimensionless pressure drop across the reservoir
 Δp = pressure drop across the reservoir, $\text{ML}^{-1}\text{T}^{-2}$, Nm^{-2}
 $\Delta \rho$ = density difference between particle and water, ML^{-3} , kg m^{-3}
 ϕ = rock porosity
 ϕ_c = cake porosity
 ω = drag force coefficient
 Λ = dimensionless total mobility

Abbreviations

PVI = pore volume injected

Subscripts

c = cake
 cr = critical
 e = electric
 g = gravity
 l = lifting
 o = oil
 p = permeate
 res = reservoir

REFERENCES

- Cheng, A. H. -D.; Benhachmi, M. K.; Halhal, D.; Ouazar, D.; Naji, A.; El Harrouni, K. Pumping Optimization in Saltwater-Intruded Aquifers. In *Coastal Aquifer Management—Monitoring, Modeling, and Case Studies*; Cheng, A. H. -D., Ouazar, D., Eds.; CRC Press: Boca Raton, 2004; pp 178–196.
- Cheng, A. H. -D.; Halhal, D.; Naji, A.; Ouazar, D. Pumping Optimization in Saltwater-Intruded Coastal Aquifers. *Water Resour. Res.* **2000**, *36*, 2155.
- Bear, J. Conceptual and Mathematical Modeling. In *Seawater Intrusion in Coastal Aquifers—Concepts, Methods, and Practices*; Bear, J., Cheng, A. H. -D., Sorek, S., Ouazar, D., Herrera, I., Eds.; Kluwer Academic Publishers: Dordrecht, 1999; pp 127–161.
- Rosenbrand, E.; Fabricius, I. L.; Kets, F. Kaolinite Mobilisation in Sandstone: Pore Plugging vs Suspended Particles. In *Thirty-Eighth Workshop on Geothermal Reservoir Engineering*; Proceedings of Stanford Geothermal Workshop, Stanford, California, Feb. 11–13, 2013; Stanford University: Stanford, CA, 2013. https://pangea.stanford.edu/ERE/db/IGAstandard/record_detail.php?id=19124.
- Rosenbrand, E.; Haugwitz, C.; Jacobsen, P. S. M.; Kjølner, C.; Fabricius, I. L. The Effect of Hot Water Injection on Sandstone Permeability. *Geothermics* **2014**, *50*, 155.
- Civan, F. *Reservoir Formation Damage: Fundamentals, Modeling, Assessment, and Mitigation*, 2nd ed.; Gulf Professional Publishing: Burlington, MA, 2007.
- Schechter, R. S. *Oil Well Stimulation*; Prentice Hall: NJ, 1992.
- Khilar, K. C.; Fogler, H. S. *Migration of Fines in Porous Media*; Kluwer Academic Publishers: Dordrecht, 1998.
- Bedrikovetsky, P. *Mathematical Theory of Oil and Gas Recovery: With Applications to ex-USSR Oil and Gas Fields*; Kluwer Academic Publishers: Dordrecht, 1990.
- Herzig, J. P.; Leclerc, D. M.; Le Goff, P. Flow of Suspensions through Porous Media—Application to Deep Filtration. *Ind. Eng. Chem.* **1970**, *62*, 8.
- Elimelech, M.; Gregory, J.; Jia, X.; Williams, R. A. *Particle Deposition and Aggregation: Measurement, Modelling, and Simulation*; Butterworth-Heinemann: Boston, 1995.
- Bradford, S. A.; Torkzaban, S. Colloid Transport and Retention in Unsaturated Porous Media: A Review of Interface-, Collector-, and Pore-Scale Processes and Models. *Vadose Zone J.* **2008**, *7*, 667.
- Torkzaban, S.; Bradford, S. A.; Walker, S. L. Resolving the Coupled Effects of Hydrodynamics and DLVO Forces on Colloid Attachment in Porous Media. *Langmuir* **2007**, *23*, 9652.
- Barkman, J. H.; Davidson, D. H. Measuring Water Quality and Predicting Well Impairment. *J. Pet. Technol.* **1972**, *24*, 865.
- Pang, S.; Sharma, M. M. A Model for Predicting Injectivity Decline in Water Injection Wells. *SPE Form. Eval.* **1997**, *12*, 194 DOI: 10.2118/28489-PA.
- Bedrikovetsky, P.; Fonseca, D. R.; da Silva, M. J.; da Silva, M. F.; Siqueira, A. G.; de Souza, A. L. S.; Furtado, C. Well-History-Based Prediction of Injectivity Decline in Offshore Waterfloods. Presented at *SPE Latin American and Caribbean Petroleum Engineering Conference and Exhibition*, Rio de Janeiro, Brazil, June 20–23, 2005; Paper SPE 93885. ISBN: 978-1-61399-006-3.
- Ochi, J.; Detienne, J. L.; Rivet, P.; Lacourie, Y. External Filter Cake Properties During Injection of Produced Waters. Presented at *SPE European Formation Damage Conference*, The Hague, Netherlands, May 31– June 1, 1999; Paper SPE 54773. ISBN: 978-1-55563-361-5.
- Ramarao, B. V.; Tien, C. Approximate Analysis of Fine-Particle Retention in the Cake Filtration of Suspensions. *Ind. Eng. Chem. Res.* **2005**, *44*, 1424.
- Tien, C. *Introduction to Cake Filtration: Analyses, Experiments and Applications*; Elsevier: Amsterdam, 2006.
- De Paiva, R. O.; Bedrikovetsky, P. G.; Furtado, C.; de Souza, A. L. V.; Siqueira, A. G. A Comprehensive Model for Injectivity Decline Prediction during PWRI. Presented at *SPE Europec/EAGE Annual Conference and Exhibition*, Vienna, Austria, June 12–15, 2006; Paper SPE 100334. ISBN: 978-1-55563-230-4.
- Zinat, F. F.; Farajzadeh, R.; Currie, P. K.; Zitha, P. L. J. Modeling of External Filter Cake Build-Up in Radial Geometry. *Pet. Sci. Technol.* **2009**, *27*, 746.
- Kalantariasl, A.; Bedrikovetsky, P. Stabilization of External Filter Cake by Colloidal Forces in a “Well-Reservoir” System. *Ind. Eng. Chem. Res.* **2014**, *53*, 930.
- King, R. W.; Adegbesan, K. O. Resolution of the Principal Formation Damage Mechanisms Causing Injectivity and Productivity Impairment in the Pembina Cardium Reservoir. Presented at *SPE Annual Technical Conference and Exhibition*, San Antonio, Texas, Oct. 5–8, 1997; Paper SPE 38870. ISBN: 978-1-55563-399-8.

- (24) Doublet, L. E.; Blasingame, T. A. Evaluation of Injection Well Performance using Decline Type Curves. Presented at *SPE Permian Basin Oil and Gas Recovery Conference*, Midland, Texas, March 27–29, 1996; Paper SPE 35205. [http://www.pe.tamu.edu/blasingame/data/0_TAB_Public/TAB_Publications/SPE_035205_\(Doublet\)_Frac_Well_Dec_TC.pdf](http://www.pe.tamu.edu/blasingame/data/0_TAB_Public/TAB_Publications/SPE_035205_(Doublet)_Frac_Well_Dec_TC.pdf).
- (25) Yuan, H.; Shapiro, A. A. A Mathematical Model for Non-Monotonic Deposition Profiles in Deep Bed Filtration Systems. *Chem. Eng. J.* **2011**, *166*, 105.
- (26) Yuan, H.; Shapiro, A. A. Modeling Non-Fickian Transport and Hyperexponential Deposition for Deep Bed Filtration. *Chem. Eng. J.* **2010**, *162*, 974.
- (27) Nunes, M.; Bedrikovetsky, P.; Newbery, B.; Paiva, R.; Furtado, C.; de Souza, A. L. Theoretical Definition of Formation Damage Zone with Applications to Well Stimulation. *J. Energy Resour. Technol.* **2010**, *132*, 033101–1.
- (28) Sharma, M. M.; Pang, S.; Wennberg, K. E.; Morgenthaler, L. N. Injectivity Decline in Water-Injection Wells: An Offshore Gulf of Mexico Case Study. *SPE Prod. Facil.* **2000**, *15*, 6 DOI: 10.2118/60901-PA.
- (29) Bedrikovetsky, P.; Siqueira, F. D.; Furtado, C. A.; Souza, A. L. S. Modified Particle Detachment Model for Colloidal Transport in Porous Media. *Transp. Porous Media* **2011**, *86*, 353.
- (30) Lake, L. W. *Enhanced Oil Recovery*; Prentice Hall: Englewood Cliffs, NJ, 1989.
- (31) Barenblatt, G. I.; Entov, V. M.; Ryzhik, V. M. *Theory of Fluids Flow through Natural Rocks*; Kluwer Academic Publishers: Dordrecht, 1990.
- (32) Farajzadeh, R.; Andrianov, A.; Zitha, P. L. J. Investigation of Immiscible and Miscible Foam for Enhancing Oil Recovery. *Ind. Eng. Chem. Res.* **2009**, *49*, 1910.
- (33) Farajzadeh, R.; Zitha, P. L. J.; Bruining, J. Enhanced Mass Transfer of CO₂ into Water: Experiment and Modeling. *Ind. Eng. Chem. Res.* **2009**, *48*, 6423.
- (34) Zhang, X.; Shapiro, A.; Stenby, E. H. Upscaling of Two-Phase Immiscible Flows in Communicating Stratified Reservoirs. *Transp. Porous Media* **2011**, *87*, 739.
- (35) Yortsos, Y. C. A Theoretical Analysis of Vertical Flow Equilibrium. *Transp. Porous Media* **1995**, *18*, 107.
- (36) Kanevskaya, R. D. Asymptotic Analysis of the Effect of Capillary and Gravity Forces on the Two-Dimensional Transport of Two-Phase Systems in a Porous Medium. *Fluid Dyn.* **1988**, *23*, 557.
- (37) Yuan, H.; Shapiro, A. A. Induced Migration of Fines during Waterflooding in Communicating Layer-Cake Reservoirs. *J. Pet. Sci. Eng.* **2011**, *78*, 618.
- (38) Coleman, T. F.; Li, Y. An Interior, Trust Region Approach for Nonlinear Minimization Subject to Bounds. *SIAM J. Optimiz.* **1996**, *6*, 418.
- (39) *MATLAB and Optimization Toolbox R2010b*; The MathWorks, Inc.: Natick, MA, 2010.
- (40) Jensen, J. L.; Lake, L. W.; Corbett, P. W. M.; Goggin, D. J. *Statistics for Petroleum Engineers and Geoscientists*; Prentice Hall: Upper Saddle River, NJ, 1997.
- (41) Honarpour, M.; Koederitz, L.; Harvey, A. H. *Relative Permeability of Petroleum Reservoirs*; CRC Press: Boca Raton, FL, 1986.
- (42) Wrobel, J. S.; Nachbin, A.; Marchesin, D. Numerical Simulation of Injectivity Loss in Stratified Reservoirs. *Commun. Numer. Methods Eng.* **2007**, *23*, 507.
- (43) Ding, D. Y. Modeling Formation Damage for Flow Simulations at Reservoir Scale. *SPE J.* **2010**, *15*, 737. DOI: <http://dx.doi.org/10.2118/121805-PA>.
- (44) Ding, D. Y. Coupled Simulation of Near-Wellbore and Reservoir Models. *J. Pet. Sci. Eng.* **2011**, *76*, 21.
- (45) Farajzadeh, R.; Andrianov, A.; Bruining, H.; Zitha, P. L. J. Comparative Study of CO₂ and N₂ Foams in Porous Media at Low and High Pressure–Temperatures. *Ind. Eng. Chem. Res.* **2009**, *48*, 4542.
- (46) Du, D. X.; Beni, A. N.; Farajzadeh, R.; Zitha, P. L. J. Effect of Water Solubility on Carbon Dioxide Foam Flow in Porous Media: An X-ray Computed Tomography Study. *Ind. Eng. Chem. Res.* **2008**, *47*, 6298.
- (47) Andrianov, A.; Farajzadeh, R.; Mahmoodi Nick, M.; Talanana, M.; Zitha, P. L. J. Immiscible Foam for Enhancing Oil Recovery: Bulk and Porous Media Experiments. *Ind. Eng. Chem. Res.* **2012**, *51*, 2214.
- (48) Mahani, H.; Sorop, T. G.; van den Hoek, P. J.; Brooks, A. D.; Zwaan, M. Injection Fall-Off Analysis of Polymer Flooding EOR. Presented at *SPE Reservoir Characterization and Simulation Conference and Exhibition*, Abu Dhabi, UAE, Oct. 9–11, 2011; Paper SPE 145125. ISBN: 978-1-61399-143-5.
- (49) Van den Hoek, P. J.; Mahani, H.; Sorop, T. G.; Brooks, A. D.; Zwaan, M.; Sen, S.; Shuaili, K.; Saadi, F. Application of Injection Fall-Off Analysis in Polymer Flooding. Presented at *SPE Europe/EAGE Annual Conference*, Copenhagen, Denmark, June 4–7, 2012; Paper SPE 154376. ISBN: 978-1-61399-204-3.
- (50) Kahrobaei, S.; Farajzadeh, R.; Suicmez, V. S.; Bruining, J. Gravity-Enhanced Transfer between Fracture and Matrix in Solvent-Based Enhanced Oil Recovery. *Ind. Eng. Chem. Res.* **2012**, *51*, 14555.
- (51) Tiab, D.; Donaldson, E. C. *Petrophysics: Theory and Practice of Measuring Reservoir Rock and Fluid Transport Properties*, 3rd ed.; Gulf Professional Publishing: Oxford, 2012.
- (52) Peters, E. J. *Advanced Petrophysics: Geology, Porosity, Absolute Permeability, Heterogeneity, and Geostatistics*; Live Oak Book: Austin, 2012; Vol. 1.